

| REPORT DOCUMENTATION PAGE | | | Form Approved OMB NO. 0704-0188 | | |
|---|-------------------|--------------------------------|---|--|---|
| <p>The public reporting burden for this collection of information is estimated to average 1 hour per response, including the time for reviewing instructions, searching existing data sources, gathering and maintaining the data needed, and completing and reviewing the collection of information. Send comments regarding this burden estimate or any other aspect of this collection of information, including suggestions for reducing this burden, to Washington Headquarters Services, Directorate for Information Operations and Reports, 1215 Jefferson Davis Highway, Suite 1204, Arlington VA, 22202-4302. Respondents should be aware that notwithstanding any other provision of law, no person shall be subject to any penalty for failing to comply with a collection of information if it does not display a currently valid OMB control number.</p> <p>PLEASE DO NOT RETURN YOUR FORM TO THE ABOVE ADDRESS.</p> | | | | | |
| 1. REPORT DATE (DD-MM-YYYY) 18-02-2013 | | 2. REPORT TYPE Final Report | | 3. DATES COVERED (From - To) 1-Feb-2009 - 31-Jan-2013 | |
| 4. TITLE AND SUBTITLE Multi-Scale Process of soil Freezing, Thawing, and Thaw-Settlement | | | 5a. CONTRACT NUMBER W911NF-08-1-0376 | | |
| | | | 5b. GRANT NUMBER | | |
| | | | 5c. PROGRAM ELEMENT NUMBER 611102 | | |
| 6. AUTHORS Radoslaw L. Michalowski and Yao Zhang | | | 5d. PROJECT NUMBER | | |
| | | | 5e. TASK NUMBER | | |
| | | | 5f. WORK UNIT NUMBER | | |
| 7. PERFORMING ORGANIZATION NAMES AND ADDRESSES University of Michigan - Ann Arbor Regents of the University of Michigan 3003 S. State St Ann Arbor, MI 48109 -1274 | | | 8. PERFORMING ORGANIZATION REPORT NUMBER | | |
| 9. SPONSORING/MONITORING AGENCY NAME(S) AND ADDRESS(ES) U.S. Army Research Office P.O. Box 12211 Research Triangle Park, NC 27709-2211 | | | 10. SPONSOR/MONITOR'S ACRONYM(S) ARO | | |
| | | | 11. SPONSOR/MONITOR'S REPORT NUMBER(S) 53315-EV.14 | | |
| 12. DISTRIBUTION AVAILABILITY STATEMENT Approved for Public Release; Distribution Unlimited | | | | | |
| 13. SUPPLEMENTARY NOTES The views, opinions and/or findings contained in this report are those of the author(s) and should not be construed as an official Department of the Army position, policy or decision, unless so designated by other documentation. | | | | | |
| 14. ABSTRACT Freezing and thawing of soils are processes that span multiple spatial scales and involve multi-physics phenomena such as phase change and multiphase flow. Of particular importance is freezing and thawing in soils susceptible to heaving. Frost heave and thawing of ice-rich soils directly affect Army operations in cold regions and the state of infrastructure. This research was focused on the study of the fundamental processes and causes of frost heaving and thaw-weakening in soils. A model describing frost heaving in soils has been developed that well captures the | | | | | |
| 15. SUBJECT TERMS Freeze-thaw cycle, frost heave, ice growth, ice lensing, phase change, soil thawing, thaw-weakening, mass transfer, heat transfer, frost susceptibility, constitutive model | | | | | |
| 16. SECURITY CLASSIFICATION OF: | | | 17. LIMITATION OF ABSTRACT UU | 15. NUMBER OF PAGES | 19a. NAME OF RESPONSIBLE PERSON Radoslaw Michalowski |
| a. REPORT UU | b. ABSTRACT UU | c. THIS PAGE UU | | | 19b. TELEPHONE NUMBER 734-763-2146 |

Report Title

Multi-Scale Process of soil Freezing, Thawing, and Thaw-Settlement

ABSTRACT

Freezing and thawing of soils are processes that span multiple spatial scales and involve multi-physics phenomena such as phase change and multiphase flow. Of particular importance is freezing and thawing in soils susceptible to heaving. Frost heave and thawing of ice-rich soils directly affect Army operations in cold regions and the state of infrastructure. This research was focused on the study of the fundamental processes and causes of frost heaving and thaw-weakening in soils. A model describing frost heaving in soils has been developed that well captures the heaving process as function of the initial and boundary conditions. The model has been extended to include the entire freeze-thaw cycle, and to predict the consequences of phase change on thaw-weakening of soils. The effects in soils with non-segregation freezing have been included in the model. Frost heaving is described by introducing an ice growth tensor, which captures the anisotropic growth of ice lenses. The evolution of the soil strength during both freezing and thawing is described through a hardening/softening plasticity model including the effects associated with freeze-thaw cycles. The model has been calibrated, it was implemented in the finite element method, and it was used to simulate boundary value problems.

Enter List of papers submitted or published that acknowledge ARO support from the start of the project to the date of this printing. List the papers, including journal references, in the following categories:

(a) Papers published in peer-reviewed journals (N/A for none)

| <u>Received</u> | <u>Paper</u> |
|-----------------|---|
| 01/27/2013 | 9.00 A. DRESCHER, R.L. MICHALOWSKI. Three-dimensional stability of slopes and excavations, Géotechnique, (01 2009): 0. doi: 10.1680/geot.8.P.136 |
| 01/27/2013 | 11.00 Radoslaw L. Michalowski. Expanding collapse in partially submerged granular soil slopes, Canadian Geotechnical Journal, (12 2009): 0. doi: 10.1139/T09-064 |
| 01/27/2013 | 10.00 Radoslaw L. Michalowski. Limit Analysis and Stability Charts for 3D Slope Failures, Journal of Geotechnical and Geoenvironmental Engineering, (04 2010): 583. doi: |
| 08/11/2011 | 2.00 Radoslaw L. Michalowski, Tabetha Martel. Stability Charts for 3D Failures of Steep Slopes Subjected to Seismic Excitation, Journal of Geotechnical and Geoenvironmental Engineering, (02 2011): 0. doi: 10.1061/(ASCE)GT.1943-5606.0000412 |
| TOTAL: | 4 |

Number of Papers published in peer-reviewed journals:

(b) Papers published in non-peer-reviewed journals (N/A for none)

| <u>Received</u> | <u>Paper</u> |
|-----------------|--------------|
|-----------------|--------------|

TOTAL:

Number of Papers published in non peer-reviewed journals:

(c) Presentations

Number of Presentations: 0.00

Non Peer-Reviewed Conference Proceeding publications (other than abstracts):

Received Paper

TOTAL:

Number of Non Peer-Reviewed Conference Proceeding publications (other than abstracts):

Peer-Reviewed Conference Proceeding publications (other than abstracts):

Received Paper

| | | |
|------------|------|--|
| 08/09/2011 | 4.00 | Radoslaw L. Michalowski, Srinivasa S. Nadukuru. Delayed increase in cone penetration resistance of sand after dynamic compaction, Second International Symposium on Computational Geomechanics (ComGeo II), Cavtat-Dubrovnik, Croatia.. 2011/04/27 00:00:00, . : , |
| 08/09/2011 | 5.00 | Srinivasa S. Nadukuru, Tabetha Martel, Radoslaw L. Michalowski. 3D analysis of steep slopes subjected to seismic excitation, Geo-Frontiers 2011, Dallas, TX.. 2011/03/13 00:00:00, . : , |
| 08/09/2011 | 6.00 | Radoslaw L. Michalowski, Srinivasa S. Nadukuru. Stress corrosion cracking and delayed increase in penetration resistance after dynamic compaction of sand, Geo-Frontiers 2011, Dallas, TX.. 2011/03/14 00:00:00, . : , |
| 08/09/2011 | 7.00 | Radoslaw L. Michalowski, Srinivasa S. Nadukuru. Post-liquefaction state of sand, stress corrosion cracking, and relaxation of deviatoric stress in previously liquefied sand bed, 5th International Conference on Earthquake Geotechnical Engineering (5ICEGE). Santiago, Chile.. 2011/01/10 00:00:00, . : , |

TOTAL: 4

Number of Peer-Reviewed Conference Proceeding publications (other than abstracts):

(d) Manuscripts

Received Paper

01/27/2013 12.00 Yao Zhang, Radoslaw L. Michalowski. Constitutive model and simulation of non-segregation freezing and thawing in soils,
16 Int. Conf. Soil Mech. Geotech. Eng. (12 2012)

02/15/2013 13.00 Yao Zhang, Radoslaw L. Michalowski. Thermal-mechanical constitutive modeling for freezing and thawing soils ,
10th International Symposium on Cold Regions Development (02 2013)

08/09/2011 3.00 Radoslaw L. Michalowski, Yao Zhang. Frost-induced heaving of soil around a culvert,
(08 2011)

08/11/2011 8.00 Radoslaw L. Michalowski, Srinivasa S. Nadukuru. Static fatigue, time effects, and delayed increase in penetration resistance after dynamic compaction of sands,
Journal of Geotechnical and Geoenvironmental Engineering (08 2011)

TOTAL: 4

Number of Manuscripts:

Books

Received Paper

TOTAL:

Patents Submitted

Patents Awarded

Awards

MTS Visiting Professor of Geomechanics, University of Minnesota, 2012

APEA Tribute Award (American Polish Engineering Association), 2010

The J.S. Braun/Braun Intertec Professorship in Science and Technology, University of Minnesota, Twin Cities, 2008

Graduate Students

| <u>NAME</u> | <u>PERCENT SUPPORTED</u> | <u>Discipline</u> |
|------------------------|--------------------------|-------------------|
| Yao Zhang | 0.75 | |
| Srinivasa Nadukuru | 0.00 | |
| FTE Equivalent: | 0.75 | |
| Total Number: | 2 | |

Names of Post Doctorates

| <u>NAME</u> | <u>PERCENT SUPPORTED</u> |
|------------------------|--------------------------|
| FTE Equivalent: | |
| Total Number: | |

Names of Faculty Supported

| <u>NAME</u> | <u>PERCENT SUPPORTED</u> | National Academy Member |
|-------------------------|--------------------------|-------------------------|
| Radoslaw L. Michalowski | 0.05 | |
| FTE Equivalent: | 0.05 | |
| Total Number: | 1 | |

Names of Under Graduate students supported

| <u>NAME</u> | <u>PERCENT SUPPORTED</u> |
|------------------------|--------------------------|
| FTE Equivalent: | |
| Total Number: | |

Student Metrics

This section only applies to graduating undergraduates supported by this agreement in this reporting period

- The number of undergraduates funded by this agreement who graduated during this period: 0.00
- The number of undergraduates funded by this agreement who graduated during this period with a degree in science, mathematics, engineering, or technology fields:..... 0.00
- The number of undergraduates funded by your agreement who graduated during this period and will continue to pursue a graduate or Ph.D. degree in science, mathematics, engineering, or technology fields:..... 0.00
- Number of graduating undergraduates who achieved a 3.5 GPA to 4.0 (4.0 max scale):..... 0.00
- Number of graduating undergraduates funded by a DoD funded Center of Excellence grant for Education, Research and Engineering: 0.00
- The number of undergraduates funded by your agreement who graduated during this period and intend to work for the Department of Defense 0.00
- The number of undergraduates funded by your agreement who graduated during this period and will receive scholarships or fellowships for further studies in science, mathematics, engineering or technology fields: 0.00

Names of Personnel receiving masters degrees

| <u>NAME</u> | |
|----------------------|----------|
| Tabetha Martel | |
| Total Number: | 1 |

Names of personnel receiving PHDs

| <u>NAME</u> | |
|----------------------|--|
| Total Number: | |

Names of other research staff

NAME

PERCENT SUPPORTED

FTE Equivalent:

Total Number:

Sub Contractors (DD882)

Inventions (DD882)

Scientific Progress

See Attachments

Technology Transfer

Multi-Scale Process of soil Freezing, Thawing, and Thaw-Settlement

Final Report to U.S. Army Research Office
(Funding W911NF-08-1-0376, Proposal Number 53315-EV)

Table of Contents

| | | |
|-----|---|----|
| 1 | Statement of the problem studied..... | 2 |
| 2 | Summary | 2 |
| 3 | Introduction and background | 2 |
| 4 | Development of the constitutive model for frost heaving | 4 |
| 4.1 | Porosity rate function for frost heave description | 4 |
| 4.2 | Simulation of the frost heave around a culvert using PRF..... | 13 |
| 4.3 | Results and Discussions | 16 |
| 5 | Elasto-plastic constitutive model for freezing and thawing soils..... | 19 |
| 5.1 | The model | 19 |
| 5.2 | Thermal-mechanical load process | 23 |
| 5.3 | Implementation and application of the model | 24 |
| 6 | Summary of the most important results | 27 |
| | References..... | 27 |

Key words:

Freeze-thaw cycle, frost heave, ice growth, ice lensing, phase change, soil thawing, thaw-weakening, mass transfer, heat transfer, frost susceptibility, constitutive model

List of Figures

| | |
|---|----|
| Figure 1. Distribution of ice fraction (Test D ₁)..... | 7 |
| Figure 2. Distribution of unfrozen water fraction (Test D ₁) | 7 |
| Figure 3. Retardation factor $\exp(-\theta_i/\theta_w)$ (Test D ₁)..... | 8 |
| Figure 4. Calibration curves for clay used in Fukuda et al. (1997) tests; each curve represents the simulation for a different thermal gradient | 8 |
| Figure 5. Comparison of the total frost heave simulated by the model developed, one other model, and the experimental tests (for different temperature gradients). 9 | 9 |
| Figure 6. Calibration curves for Fukuda et al. (1997) tests with different overburden pressure (revised model) | 10 |
| Figure 7. Comparison of the total frost heave simulated by the model developed, one other model, and the experimental tests (for different overburden pressures) 10 | 10 |
| Figure 8. JGST freezing process | 11 |
| Figure 9. Test data and calibration curve for unfrozen water content in Alaskan silt | 12 |
| Figure 10. Calibration of the model with JGST-freezing test for Alaskan silt | 13 |
| Figure 11. Geometry and mesh of the model culvert..... | 13 |
| Figure 12. The annual air temperature variation in Aniak, AK, 1961 – 1962 | 14 |
| Figure 13. (a) Below-ground temperature in Aniak, AK, 1952 – 1953 (after Aitken and Fulwider, 1962), (b) Initial temperature profile for 1D simulation | 15 |
| Figure 14. Temperature regimes for 1D simulations | 15 |
| Figure 15. Frost heave simulation results (1-D) | 15 |
| Figure 16. Initial temperature distribution at $t = 0$ | 16 |
| Figure 17. (a) Temperature distribution after 37 days, and (b) frost heave contour..... | 17 |
| Figure 18. (a) Temperature distribution after 100 days, and (b) frost heave contour..... | 17 |
| Figure 19. (a) Temperature distribution after 46 days, and (b) frost heave contour (culvert with outside thermal insulation around the circumference, $\lambda = 0.02 \text{ W/(m } ^\circ\text{C)}$). | 18 |
| Figure 20. (a) Temperature distribution after 100 days, and (b) frost heave contour (culvert with outside thermal insulation around the circumference, $\lambda = 0.02 \text{ W/(m } ^\circ\text{C)}$). | 18 |
| Figure 21. (a) Freeze-thaw thermal loading path in $v\text{-ln}(p)$ plane; (b) “pseudo preconsolidation pressure” changing along BD due to increasing pore ice ratio | 21 |
| Figure 22. Freeze-thaw cycle and load path with corresponding yield curves | 24 |
| Figure 23. Calibration of preconsolidation stress for frozen soil vs temperatures | 25 |
| Figure 24. Boundary condition on top of the soil column | 26 |
| Figure 25. Temperature distribution at $t = 0$ and $t = 300 \text{ h}$ | 26 |
| Figure 26. Compression for element #18 (a) and element #4 (b) | 27 |

1 Statement of the problem studied

Phenomena associated with freeze-thaw cycles in soils are not fully understood, which hinders the development of efficient models for model-based simulations. Both the formation of ice lenses during freezing and soil weakening during thawing were studied. In particular, a porosity growth function was considered with the goal of developing a frost heave model, and a plasticity-based solid model with hardening and softening governed by ice content was studied to model increase in strength during freezing and weakening during thawing.

2 Summary

Thermal effects in soils are relevant to both Army and civilian operations, particularly in the regions of seasonal freezing and permafrost. The significance of thermal processes in soils may be amplified if the current trends in climate changes continue. Of problems that require attention are the frost heave and thaw weakening of soils during freeze-thaw cycles. Both have been studied with the goal of developing a mathematical description that could be used successfully in model-based simulations.

The progress in the description of frost heave has been hindered by the lack of understanding of the factors behind development of cryogenic suction in freezing soils. From the numerical standpoint, on the other hand, the difficulties lay in the fact that some of the crucial parameters in the freezing zone evolve by orders of magnitude (e.g., hydraulic conductivity), and evaluation (calibration) of those parameters are quite difficult. In modeling, this problem was overcome by introducing a concept of *porosity rate function*, which allows eliminating hydraulic conductivity from the model by introducing a porosity growth tensor, which was successfully calibrated.

The second, equally important issue is that of the evolution of strength of the soil during freezing and thawing. A model was developed based on hardening plasticity, with ice content and specific volume being the principal parameters responsible for hardening and softening of the soil. The models were used with success in simulations of freezing and thawing of frost-susceptible soils.

3 Introduction and background

Cold regions, including permafrost and seasonal freezing areas constitute a large portion of Earth's surface. In the northern hemisphere, more than 20% of land surface is occupied by permafrost, whereas more than 50% experiences seasonal freezing and thawing. Frost action in soils involving frost heaving and thaw settlement is commonly seen in seasonal freezing areas rendering built infrastructure vulnerable to damage. Broken communication channels, damaged lifelines, broken pipelines, malfunctioning utilities, cracked pavements, jacked up bridge foundations, tilted structures, are all examples of damage suffered from frost action. Long-term paleographic records indicate an on-going

warming of the climate, which has resulted in thawing of portions of the permafrost area. The increase in permafrost temperature leads to thickening of the active layer (upper crust layer where active freezing-thawing cycles occur), leading to extensive settlement of the ground surface causing damage to infrastructure. Understanding how the soil behaves upon freezing and thawing has the potential of changing the operation practices and design philosophies, and developing methods to alleviate the damages.

Various soils experiencing freezing and thawing may exhibit dramatically different behaviors. A good portion of silty soils and clays are characterized by susceptibility to frost heaving. This process is caused by transfer of moisture from unfrozen layers of soil into the freezing zone, driven by gradient in *cryogenic suction*, and freezing to form segregated ice referred to as *ice lenses*. The zone where this process occurs is often called the *frozen fringe*. The frost heave of a frost-susceptible soil could be more than 20% of the thickness of the frozen layer, and it depends on the rate of freezing front propagation through this layer. Upon thawing, the thaw settlement could be larger or smaller than the displacement caused by frost heave, depending on whether the soil was normally consolidated (*NC*) or over-consolidated (*OC*) prior to freezing.

Thawing of a frozen *NC* soil in its first freeze-thaw cycle could cause a settlement larger than the heave induced during the freezing phase. However, some heave could remain in an *OC* soil subjected to its first freeze-thaw cycle. Artificial ground freezing applied in soft soil construction (tunneling, excavations), and pipelines transporting chilled media through unfrozen soil, are examples of circumstances where soil may be subjected to its first freeze-thaw cycle.

For a non-frost-susceptible soil, such as sand or gravel, no ice segregation will take place during freezing. Pore ice will be formed due to the phase change of the water in the pores. While the transfer of moisture can still occur due to the thermal gradient, ice lenses do not form, and the macroscopic deformation of the soil mixture (mineral, ice, water, air) upon freezing is owed to expansion of freezing water. This expansion may be fully accommodated by pores in unsaturated soils, but it will cause macroscopic deformation in water-saturated soils

In addition to the deformation induced by the freezing process in soils, the strength gain (hardening) during freezing and soil weakening (softening) during thawing, are important concerns in cold regions operations. Experimental data indicates that an increase in strength occurs in both the frost-susceptible and non-frost-susceptible soils as they freeze. A reduction in strength is then expected upon thawing.

Constitutive models describing changes in strength caused by freeze-thaw cycles have not been developed, though some efforts have been published recently (e.g., Lai et al., 2009, Wei et al., 2011, Shastri and Sanchez, 2012). These models assume elasto-plastic behavior with account for viscous properties of ice (creep); they are based on continuum approach, and are customized for one type of the frozen soil. Changes of the soil components upon freezing and thawing, and the corresponding changes in strength, are not addressed by these models.

The model developed in this research contains two parts: a revised porosity rate model for frost heaving and an elasto-plastic constitutive model with evolution of soil strength caused by freezing and thawing. The constitutive model developed is capable of addressing freezing and thawing effects, it captures the deformation behavior, and describes the evolution of strength in the soil subjected to loading and thermal changes, including phase change. The model is based on the *critical state* concept and it is formulated by introducing the influence of *ice ratio* into the hardening/softening plasticity framework. The model was implemented in the finite element method, and boundary value problems were successfully simulated.

4 Development of constitutive model for frost heaving

4.1 Porosity rate function for frost heave description

Frost heave is caused by the growth of ice lenses, and the porosity rate function describes the average growth of ice in a soil volume. This model was found to be very effective in simulations of frost heave processes. A great advantage of this model is a relatively small number of parameters needed to describe the process of frost heave. The model assumes the soil to be saturated, and the soil skeleton to behave as an elastic solid. An early proposal of a porosity rate function, central to this model, was suggested in Michalowski (1993), and it was modified later by Michalowski and Zhu (2006). The porosity growth in this model is described by the *porosity rate tensor*

$$\dot{n}_{ij} = \dot{n} \varepsilon_{ij}^f \quad (1)$$

where ε_{ij}^f is a unit strain tensor that maps the ice volume increase into anisotropic growth consistent with the growth of ice lenses, and \dot{n} is a scalar function representing porosity growth

$$\dot{n} = \dot{n}_m \left(\frac{T - T_0}{T_m} \right)^2 \cdot e^{1 - \left(\frac{T - T_0}{T_m} \right)^2} \cdot \frac{\left| \frac{\partial T}{\partial l} \right|}{g_T} \cdot e^{-\frac{|\bar{\sigma}_{kk}|}{\zeta}} \quad (2)$$

Notation: \dot{n} is the porosity rate ($\partial n / \partial t$), T is the temperature of the soil ($^{\circ}\text{C}$), and $\bar{\sigma}_{kk}$ is the first invariant of the stress tensor in the frozen soil (zero if tension). Parameters \dot{n}_m and T_m are the maximum porosity rate and the temperature ($^{\circ}\text{C}$) at which that maximum porosity rate occurs, respectively; T_0 is the freezing temperature of water; \dot{n}_m is determined at well-defined temperature gradient g_T ; ζ is a material parameter defining stress dependency. The quotient $\left| \frac{\partial T}{\partial l} \right| / g_T$ indicates linear relationship of the porosity rate to the temperature gradient in the heat flow direction. The term $\exp(-|\bar{\sigma}_{kk}| / \zeta)$ is a

retardation function: frost heave can be significantly reduced by the compressive stress in the direction of heat flow, with some contribution of the normal stresses in the other two perpendicular directions (parameter ζ was calibrated for specific clay). A porosity threshold of 0.75 was introduced, past which further heave ceases, to indicate the fact that the frost heave stops, or reduces to an insignificant rate, after the freezing front reaches a steady-state location (Fukuda et al., 1997).

A modification of this model was proposed to make it more realistic in describing the influence of stress state and the soil components (soil skeleton, unfrozen water and ice) to the frost heave process. The modified porosity rate function has the following form

$$\dot{n} = \dot{n}_m \left(\frac{T - T_0}{T_m} \right)^2 \cdot e^{1 - \left(\frac{T - T_0}{T_m} \right)^2} \cdot \frac{\left| \frac{\partial T}{\partial l} \right|}{g_T} \cdot e^{-\frac{|\bar{\sigma}_l|}{\zeta}} \cdot e^{-\frac{\theta_i}{\theta_w}} \quad (3)$$

where $\bar{\sigma}_l$ is the stress component in the heat flow direction, and θ_i and θ_w are the volumetric fractions of ice and unfrozen water, respectively.

The first invariant of the total stress tensor in soil $\bar{\sigma}_{kk}$ was replaced by the stress in the heat flow direction $\bar{\sigma}_l$. The reason for that modification is that the ice lenses tend to grow in the heat flow direction and it is the stress component in that direction that inhibits the heave.

In frozen silt and clay, only a portion of liquid water turns into solid phase at the freezing point, and the rest remains in a liquid state at the temperature well below freezing. A 3-parameter function (Michalowski 1993) is chosen here to describe the unfrozen water content in the frozen soil

$$w = w^* + (\bar{w} - w^*) e^{a(T - T_0)} \quad (4)$$

The calibration for clay in Fukuda et al. (1997) tests results in the following set of parameters: $w^* = 0.058$, $\bar{w} = 0.285$, $T_0 = 0^\circ\text{C}$, and $a = 1.6$. In the following, the modified porosity rate function is calibrated for clay based on an extensive set of tests by Fukuda et al. (1997).

The clay tested by Fukuda et al. was saturated, with the initial porosity of 0.427, and specific gravity of 2.62. The density of the soil was as $1,927 \text{ kg/m}^3$, the Young's modulus and Poisson's ratio were taken as $E = 11.2 \text{ MPa}$ and $\mu = 0.3$ for both frozen and unfrozen soil. The typical values of thermal properties for soil particles, water and ice are listed in Table 1. These values are used in both numerical calibration tests and in the numerical simulations of boundary value problems.

Table 1 Thermal properties of clay soil constituents (after Williams and Smith, 1989)

| | Density $\rho(\text{kg/m}^3)$ | Mass heat capacity $c(\text{J}/(\text{kg}\cdot^\circ\text{C}))$ | Volumetric heat capacity $C(\text{J}/(\text{m}^3\cdot^\circ\text{C}))$ | Latent heat $L(\text{J}/\text{kg})$ | Thermal Conductivity $\lambda(\text{W}/\text{m}^3\cdot^\circ\text{C})$ |
|----------------------------------|----------------------------------|---|--|---|--|
| Soil particles (clay mineral) | 2620 | 900 | $2.36\cdot 10^6$ | -- | 2.92 |
| Water | 1000 | 4180 | $4.18\cdot 10^6$ | $3.33\cdot 10^5$ | 0.56 |
| Ice | 917 | 2100 | $1.93\cdot 10^6$ | | 2.24 |

The porosity rate function in equation (3) was implemented in the FEM system ABAQUS, with a porosity growth tensor and thermal conservation equations which can be found in Michalowski and Zhu (2006). Then the implemented model was used to simulate a set of soil freezing tests performed by Fukuda et al. (1997). The specimens were cylindrical, 100 mm in diameter with initial height of 70 mm. The initial and boundary conditions for the tests performed under constant load are listed in Table 2. All these tests had ramped temperatures. The frost heave parameters for the particular clay used in Fukuda et al. (1997) tests were found to be: $T_m = -0.74^\circ\text{C}$, $\dot{n}_m = 1.88\cdot 10^{-5}\text{ s}^{-1}$, $g_T = 100^\circ\text{C}/\text{m}$, and $\zeta = 0.42\text{ MPa}$.

Table 2 Boundary/initial conditions for tests by Fukuda et al. (1997)

| Ramped Freezing Tests (dT/dl) | | Warm plate (top) ($^\circ\text{C}$) | Cold plate (bottom) ($^\circ\text{C}$) | Overburden pressure (kPa) |
|----------------------------------|-------|--|---|------------------------------|
| A | 0.095 | $7-0.042t^*$ | $-0.042t$ | 25 |
| B | 0.070 | $5-0.042t$ | $-0.042t$ | 25 |
| C | 0.061 | $4-0.042t$ | $-0.042t$ | 25 |
| D ₁ | 0.045 | $3-0.042t$ | $-0.042t$ | 25 |
| D ₂ | | | | 150 |
| D ₃ | | | | 300 |
| D ₄ | | | | 400 |
| D ₅ | | | | 600 |
| E | 0.035 | $2-0.042t$ | $-0.042t$ | 25 |

* t =time (in hours), total testing time 47hrs.

To illustrate the role term $e^{-\frac{\theta_i}{\theta_w}}$ plays in the porosity rate function, the volumetric content of ice, water and the value of the retardation coefficient in the simulated test D₁ (see Table 2) are plotted in Figure 1 through Figure 3. As the ice fraction increases, the term $e^{-\frac{\theta_i}{\theta_w}}$ decreases. This is the effect that allowed elimination of shut-off porosity threshold from the earlier model.

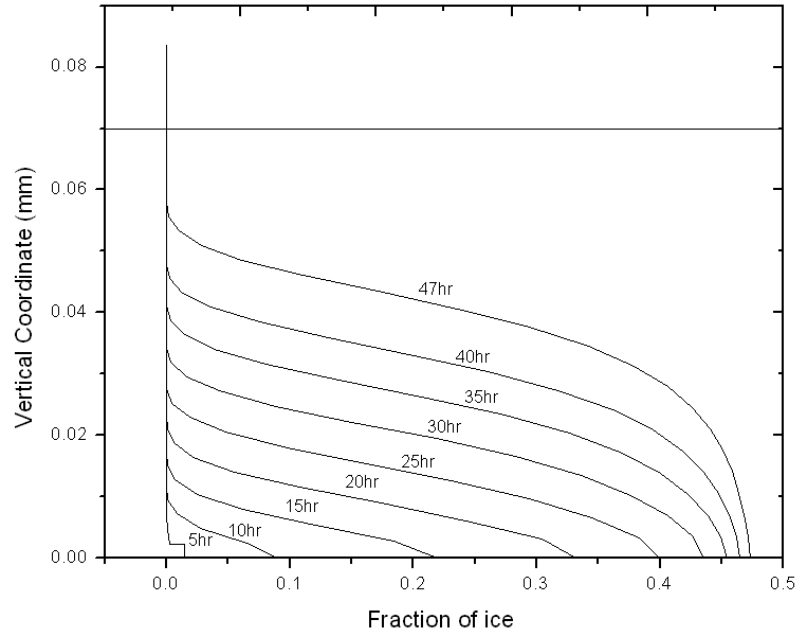


Figure 1. Distribution of ice fraction (Test D₁)

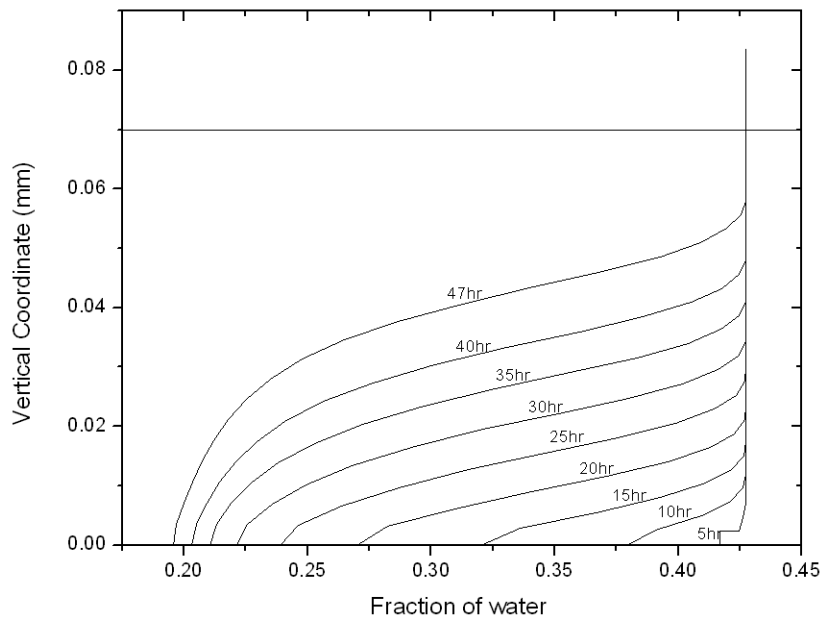


Figure 2. Distribution of unfrozen water fraction (Test D₁)

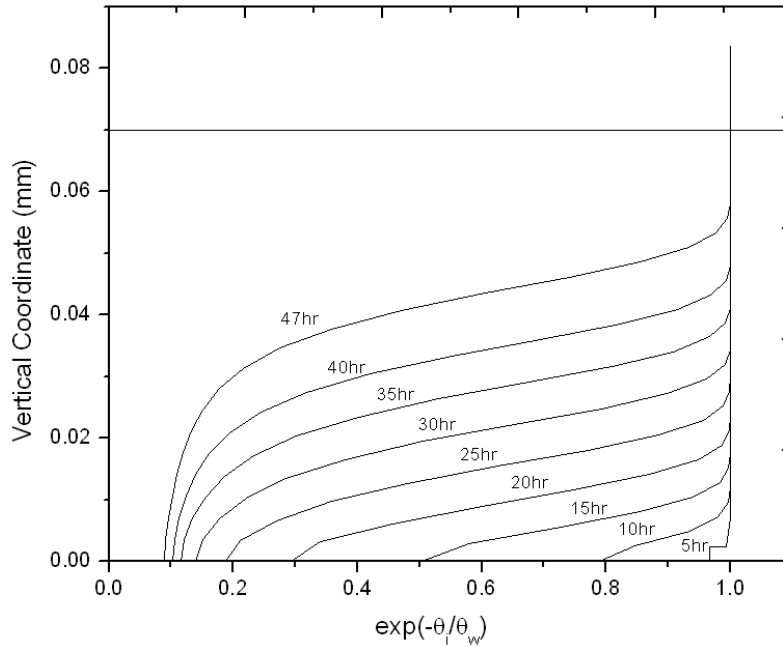


Figure 3. Retardation factor $\exp(-\theta_i/\theta_w)$ (Test D₁)

The calibration (curve fitting) process was performed first using tests with different temperature gradients (A, B, C, D₁, E in Table 2), and then the influence of stress was calibrated using the tests with different overburden load (D₁ to D₅ in Table 2). The first family of the calibration curves (dependence on the thermal gradient) is shown in Figure 4.

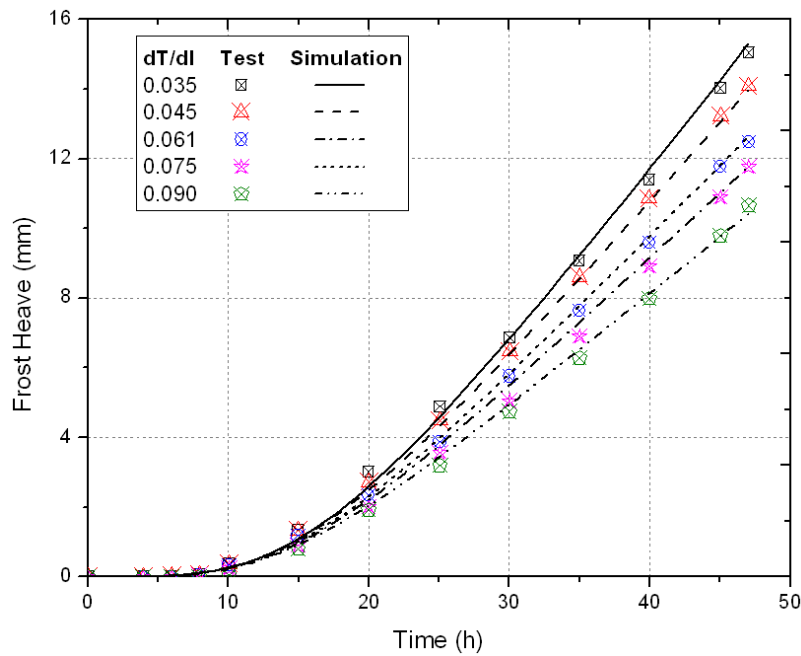


Figure 4. Calibration curves for clay used in Fukuda et al. (1997) tests; each curve represents the simulation for a different thermal gradient

Comparison of the heave magnitudes from the best calibration (curve fitting) effort is illustrated in Figure 5.

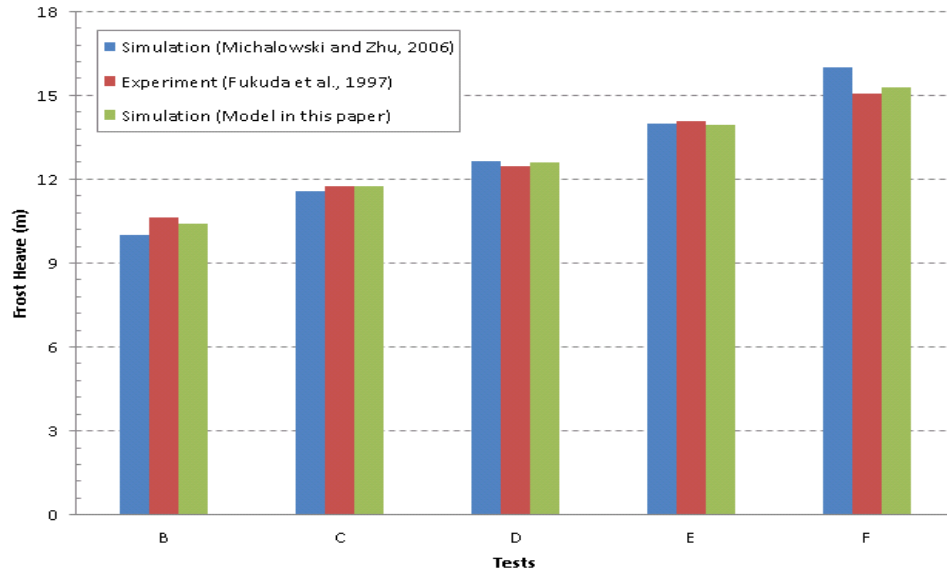


Figure 5. Comparison of the total frost heave simulated by the model developed, one other model, and the experimental tests (for different temperature gradients)

The respective graphs from the calibration effort with the tests of varied overburden pressure are shown in Figure 6 and Figure 7.

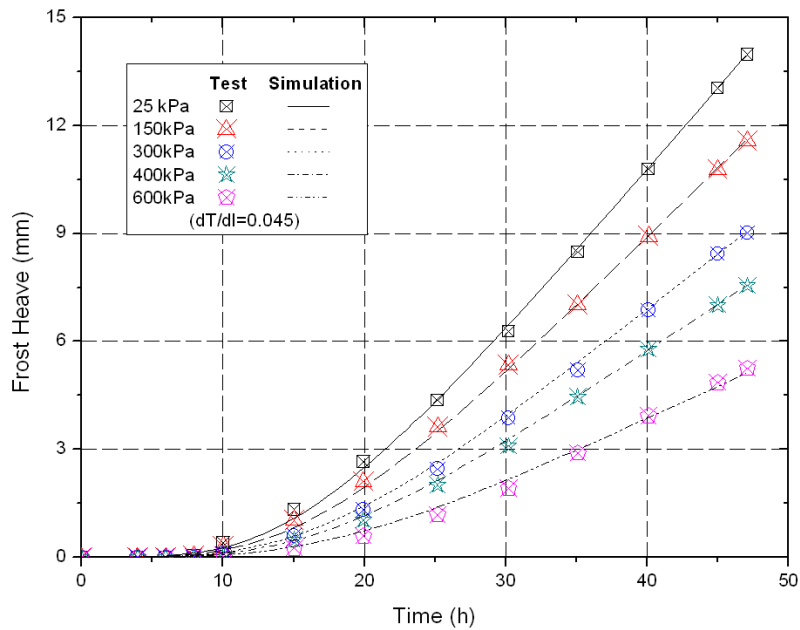


Figure 6. Calibration curves for Fukuda et al. (1997) tests with different overburden pressure (revised model)

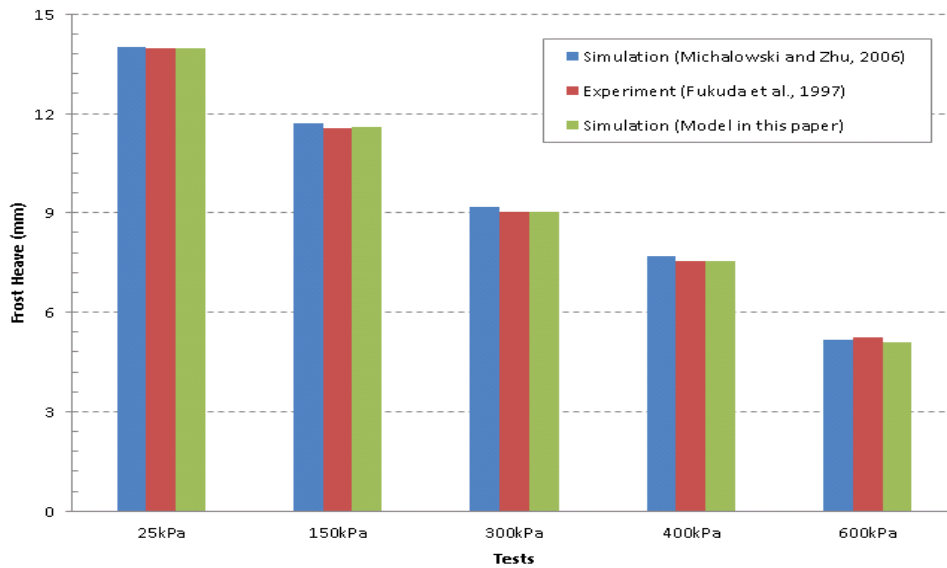


Figure 7. Comparison of the total frost heave simulated by the model developed, one other model, and the experimental tests (for different overburden pressures)

The Root-Mean-Square Error (RMSE) is 0.0098 to 0.0206 for calibration with different temperature gradients, and 0.0052 to 0.0069 for calibration with respect to different overburden load.

Additional calibration was performed for Alaskan silt, based on tests performed according to Japanese Geotechnical Standard Test (JGST) by Kim (2011) at the University of Alaska, Fairbanks. JGST freezing test is the standard test method for obtaining frost susceptibility in Japan (Japan Geotechnical Society 2003), which requires the temperature of the warm boundary to remain constant slightly above 0 °C, whereas the temperature of the cold boundary is gradually reduced at a constant rate. Figure 8 illustrates the temperature change for a JGST freezing test.

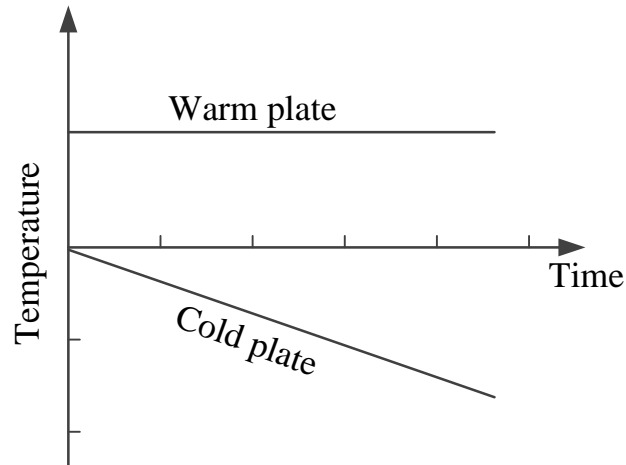


Figure 8. JGST freezing process

The set of tests selected to calibrate the model are JGST9 to JGST12 for Alaska silts (Kim, 2011). The test conditions are summarized in Table 3. Since the set of JGST frost heave tests selected contains effects of both different overburden pressure and temperature gradient, parameters in porosity rate function can be determined.

Table 3 Conditions for JGST tests

| Test No. | Linear reduction of top pedestal temperature (°C) | Average bottom pedestal temperature (°C) | Operation time (h) | Overburden pressure (kPa) |
|----------|--|---|--------------------|---------------------------|
| JGST- 9 | -0.26 → -3.93 | 0.31 | 40 | 30 |
| JGST-10 | -0.19 → -3.80 | 0.16 | | 40 |
| JGST-11 | -0.26 → -3.86 | 0.32 | | 60 |
| JGST-12 | -0.24 → -3.84 | 0.29 | | 80 |

The calibration for unfrozen water content in Alaskan silt results in the following set of parameters: $w^* = 0.813$, $\bar{w} = 0.325$, $T_0 = 0$ °C, and $a = 6.0$.

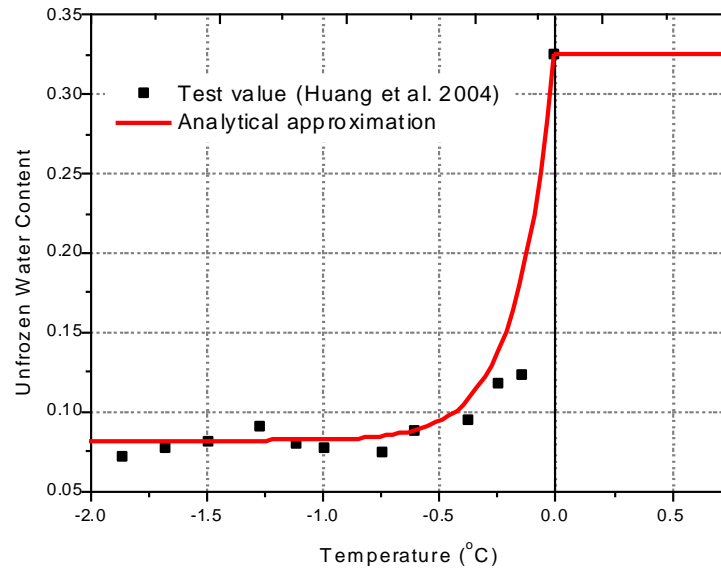


Figure 9. Test data and calibration curve for unfrozen water content in Alaskan silt

The Alaskan silt was saturated, with the initial porosity of 0.47, and specific gravity of 2.62. The density of the soil was $1,923 \text{ kg/m}^3$, the Young's modulus and Poisson's ratio were taken as $E = 11.2 \text{ MPa}$ and $\mu = 0.3$ for both frozen and unfrozen soil. The properties for Alaskan silt particles were measured by Kim (2011) and are listed in Table 4. Properties for ice and water are given in Table 1.

Table 4 Thermal properties of Alaska silt soil particles (Kim, 2011)

| | Density $\rho(\text{kg/m}^3)$ | Mass heat capacity $c(\text{J}/(\text{kg} \cdot ^\circ\text{C}))$ | Volumetric heat capacity $C(\text{J}/(\text{m}^3 \cdot ^\circ\text{C}))$ | Thermal Conductivity $\lambda(\text{W}/\text{m}^3 \cdot ^\circ\text{C})$ |
|----------------------------------|----------------------------------|---|--|--|
| Soil particles (clay mineral) | 2746 | 800 | $2.20 \cdot 10^6$ | 2.92 |

The calibration with Kim (2011) is illustrated in Figure 10. The parameters obtained from calibration are: $T_m = -0.20 \text{ }^\circ\text{C}$, $\dot{n}_m = 1.80 \cdot 10^{-5} \text{ s}^{-1}$, $g_T = 100 \text{ }^\circ\text{C}/\text{m}$, and $\zeta = 0.058 \text{ MPa}$.

These parameters will be used in a simulation to illustrate the application of the model, and to reveal an interesting phenomenon of a frost-induced heave around a culvert.

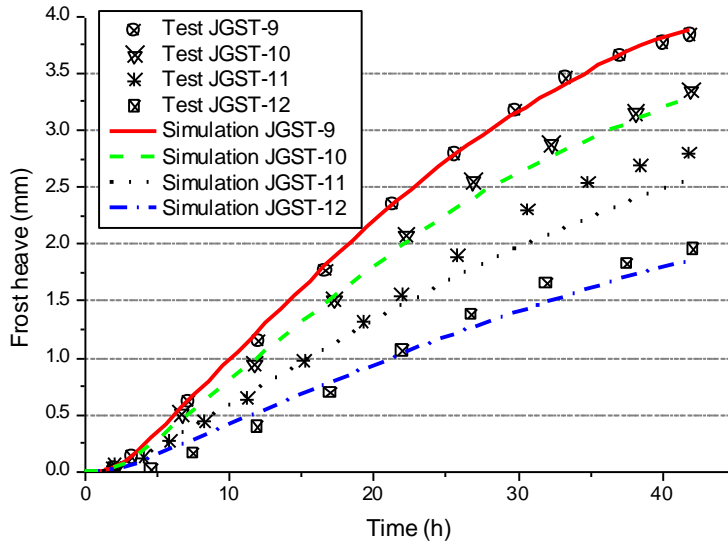


Figure 10. Calibration of the model with JGST-freezing test for Alaskan silt

4.2 Simulation of the frost heave around a culvert using PRF

To illustrate applicability of the model, simulations of freezing of an unpaved road above a culvert in frost susceptible soil were carried out. The model was implemented in the FEM system ABAQUS. The geometry of the boundary value problem and the finite element mesh of the culvert and the surrounding soil are shown in Figure 11. The top of the culvert in this simulation is located 1.0 m below the ground surface. The external diameter of it is 1.0 m and its wall thickness is 10.0 mm. The material of the culvert is steel, and a perfect bonding with soil (ad-frozen interface) is modeled. The simulations were performed for the boundary conditions consistent with Alaska climate at Aniak, AK.

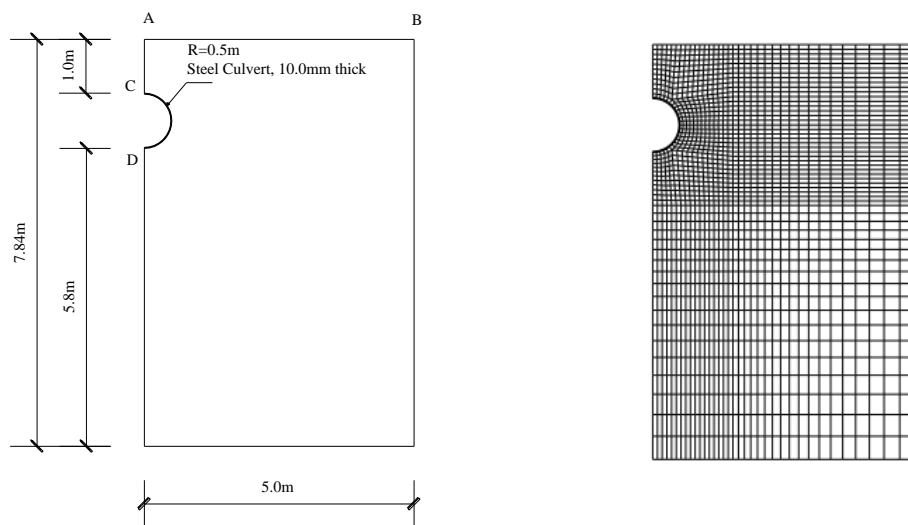


Figure 11. Geometry and mesh of the model culvert

More details on this simulation can be found in Zhang and Michalowski (2012). The data of daily air temperature change in Aniak, AK, from year 1961 to 1962 was obtained from National Climate Data Center and it is shown in Figure 12. The trend of the seasonal temperature change is very clear and regular. The highest temperature is around 20°C and the lowest temperature is around -40°C. Freezing temperatures last for about 2/3 of a year. When freezing starts, the temperature drops down from above zero to about -30°C in about 3 months. The mean daily temperature amplitude (defined as the difference between the peak and the mean daily value) is about 10°C, although it happens sometimes to reach as much as 20°C.

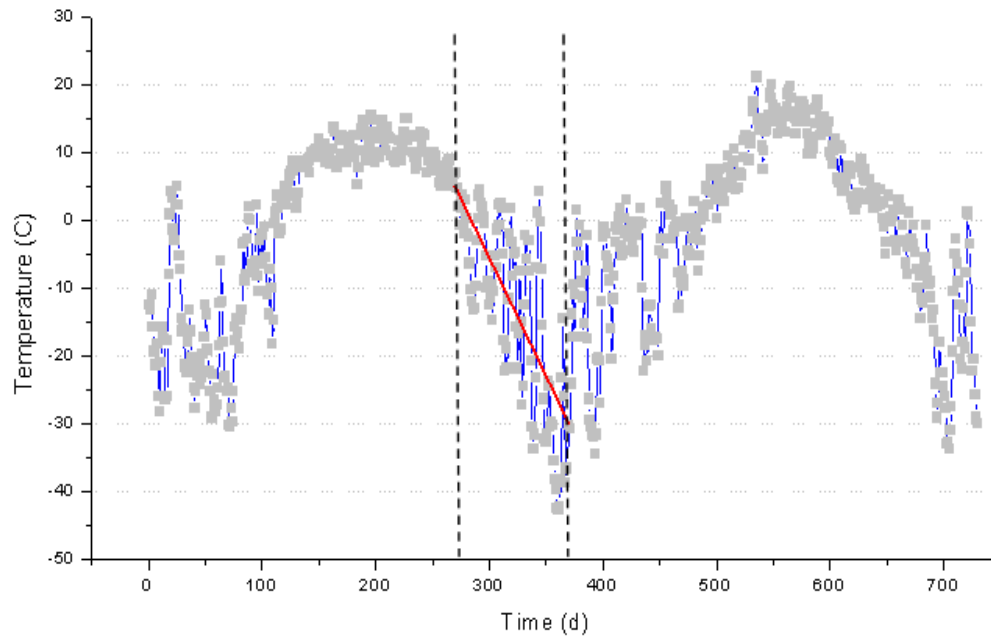


Figure 12. The annual air temperature variation in Aniak, AK, 1961 – 1962 (National Climate Data Center)

The ground temperature in Alaska was monitored by U.S. Army Cold Regions Research and Engineering Laboratory (CRREL) researchers during the year 1947 to 1958 at several locations. The ground temperature in Aniak, AK, was reported and the temperature profile below the ground surface is shown in Figure 13(a) from the end of freezing season in 1952 until the middle of the freezing season in 1953 (Aitken and Fulwider, 1962). This figure indicates small variations of temperature at about 4 m (12 ft) below the ground surface, and the temperature is nearly constant at about 3°C (37°F) at depth of about 7 m (22 ft).

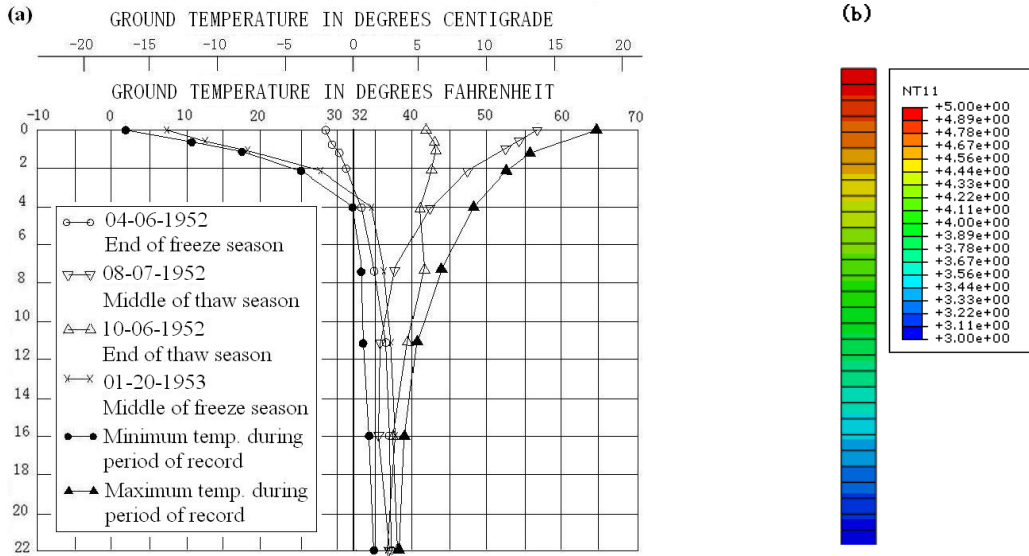


Figure 13. (a) Below-ground temperature in Aniak, AK, 1952 – 1953 (after Aitken and Fulwider, 1962), (b) Initial temperature profile for 1D simulation

A portion of the temperature function from early October, 1952 (day 270) to early January, 1953 (day 370), a total 100 days (shown in Figure 12) were used in the simulation. The bottom boundary of the model in Figure 11 is assumed to have a constant temperature of 3°C. The thermal boundaries between air and soil, air and culvert are simulated using a Fourier boundary condition

$$\lambda \nabla T = h_c (T_{air} - T) \quad (5)$$

where λ and h_c are the soil heat conductivity and convective heat transfer coefficient, T is soil temperature and T_{air} is the ambient temperature.

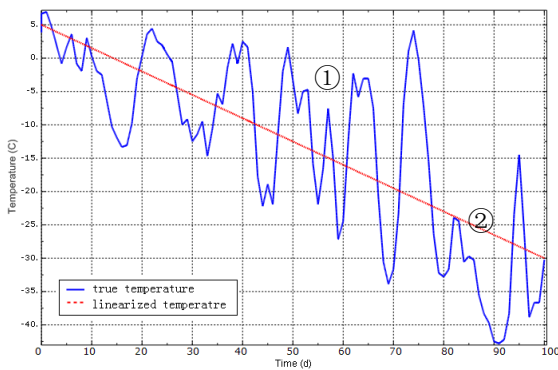


Figure 14. Temperature regimes for 1D simulations

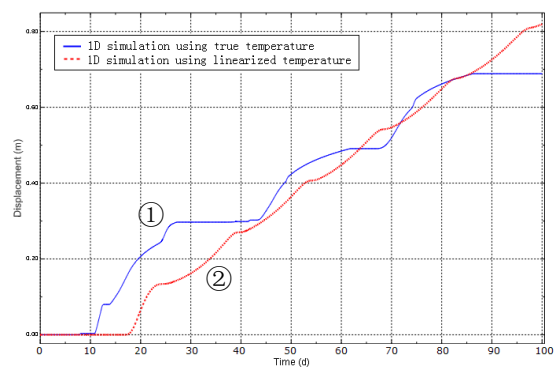


Figure 15. Frost heave simulation results (1-D)

One-dimensional soil freezing tests were simulated first, using the true temperature data and the linearized temperature change (curve 1 and 2 in Figure 14). These temperature

functions are used as the boundary conditions at the top of a seven-meter column in 1D simulation, whereas the bottom temperature is kept at 3°C. The initial temperature distribution for the 1D simulation is shown in Figure 13(b). The 1D frost heave simulation results are shown in Figure 15. The results indicate that the 1D frost heave simulated using the linearized temperature function is quantitatively similar to that from simulation with the true temperature.

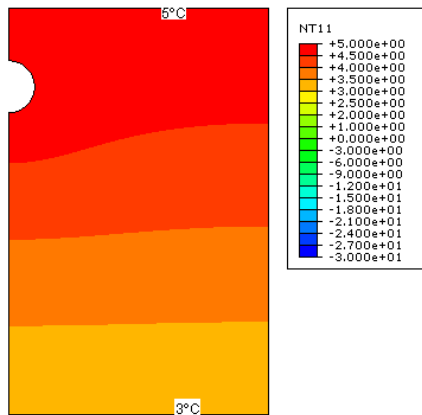


Figure 16. Initial temperature distribution at $t = 0$.

The linearized air temperature function was used in the culvert simulation. At time $t = 0$, the temperature of the ground surface and the temperature inside the culvert are set to be 5°C. Then the ambient temperature drops down to -30°C in 100 days (shown in Figure 15 line 2). The temperature at the base of the model (bottom boundary) is kept constant at 3°C. The initial temperature distribution is shown in Figure 16.

The values of the parameters in the porosity rate function used here were taken from calibration based on tests done by Kim (2011) and they were given in the earlier Section describing the porosity rate function. However, to simulate the soil that is less frost susceptible, the value of \dot{n}_m was set to be 10% of the value from the calibration: $\dot{n}_m = 1.80 \cdot 10^{-6} \text{ s}^{-1}$

The soil is assumed to be saturated, with the initial porosity of 0.47, and specific gravity of 2.62. The density of the soil was $1,923 \text{ kg/m}^3$, the Young's modulus and Poisson's ratio were taken as $E = 11.2 \text{ MPa}$ and $\mu = 0.3$ for both frozen and unfrozen soil. The thermal parameters were taken from Williams and Smith (1989) and Selvadurai et al. (1999). The thermal conductivities for soil particles, water, and ice were taken as 2.92, 0.56, and 2.24 $\text{W}/(\text{m } ^\circ\text{C})$. The heat capacities for soil particles, water, and ice were set to 800, 4180, and 2100 $\text{J}/(\text{kg } ^\circ\text{C})$. The latent heat of fusion of water is $3.33 \cdot 10^5 \text{ J/kg}$. The properties of the culvert steel were taken as: thermal conductivity 36 $\text{W}/(\text{m } ^\circ\text{C})$, mass heat capacity 477.3 $\text{J}/(\text{kg } ^\circ\text{C})$, and density $7,800 \text{ kg/m}^3$.

In addition to simulating the boundary value problem defined in Figure 11, an influence of using culvert insulation on the frost heave resulting from the same thermal boundary conditions was studied. A 10 mm thick layer of insulation with a heat conductivity of $\lambda = 0.02 \text{ W}/(\text{m } ^\circ\text{C})$ was placed around the outside perimeter of the culvert. The density of the insulation is 50 kg/m^3 , the Young's modulus and Poisson's ratio were taken as $E = 10.0 \text{ MPa}$ and $\mu = 0.3$, and the heat capacity was 2,000 $\text{J}/(\text{kg } ^\circ\text{C})$.

4.3 Results and discussions

The results of frost heave simulation around a culvert are shown in Figure 17 and Figure 18. At first, a “bump” is formed at the surface directly above the culvert; this bump

reaches its maximum after 37 days. Thereafter, the bump stops growing and turns into a “dip”; the displacements after 100 days are shown in Figure 18.

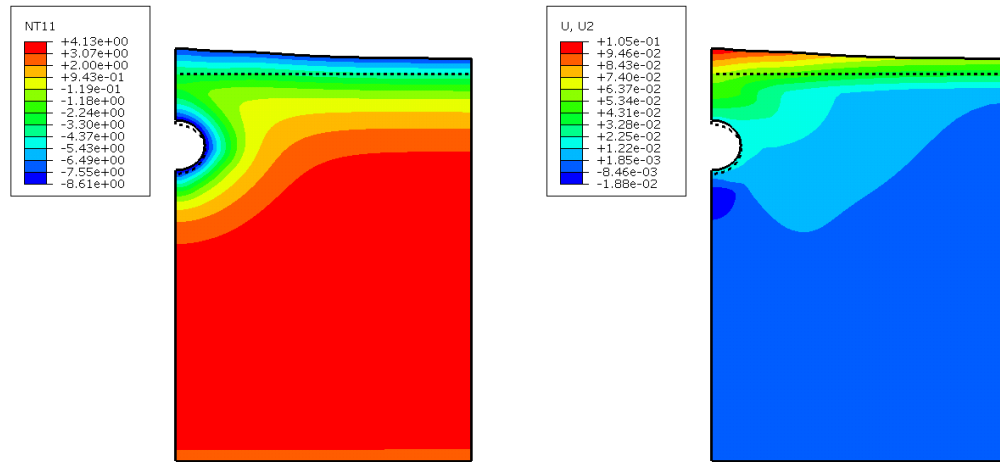


Figure 17. (a) Temperature distribution after 37 days, and (b) frost heave contour.

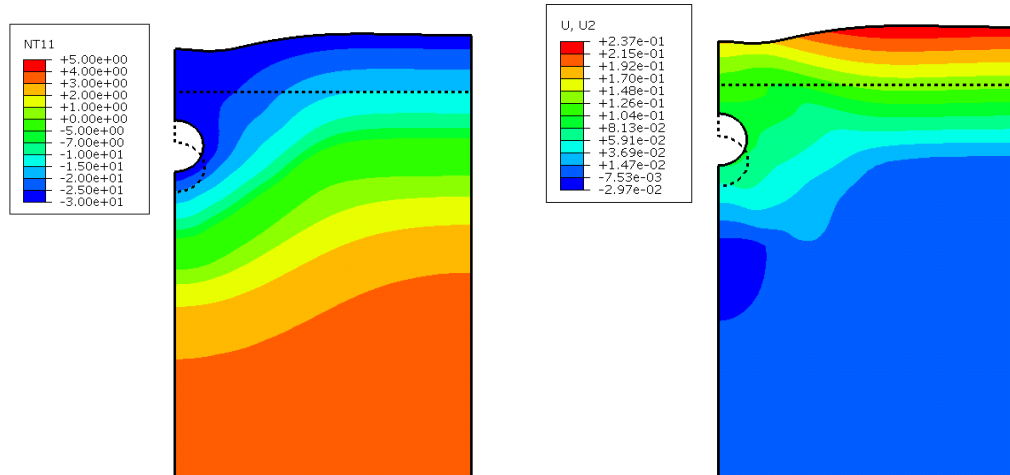


Figure 18. (a) Temperature distribution after 100 days, and (b) frost heave contour.

When the air temperature drops below freezing, two freezing fronts propagate into the soil directly above the culvert: one down from the surface, and the second one up from the culvert. If the soil is frost-susceptible, the heave process (ice lens growth) will occur in the soil. Initially, this process is particularly intense above the culvert, as this portion of the soil has the freezing front propagating both from the surface of the soil and from the culvert side. The resulting outcome is a bump on the surface. If the freezing temperature continues, the bump will continue to grow until all soil above the culvert becomes all frozen. After that, the heave of the area above the culvert slows down (or drops down to insignificant rate), but the heave in regions further away from the culvert continues, which eventually results in a “dip” in the surface above the culvert.

The key factor that determines the profile of the surface above the culvert is the boundary condition. If the freezing temperature continues only for a short period, a “bump” will form on the ground surface, whereas if the freezing temperature persists for a long time, a “depression” is likely to occur. While the former is confirmed by observations (Andersland and Ladanyi 2004) the latter is a hypothetical long-term outcome.

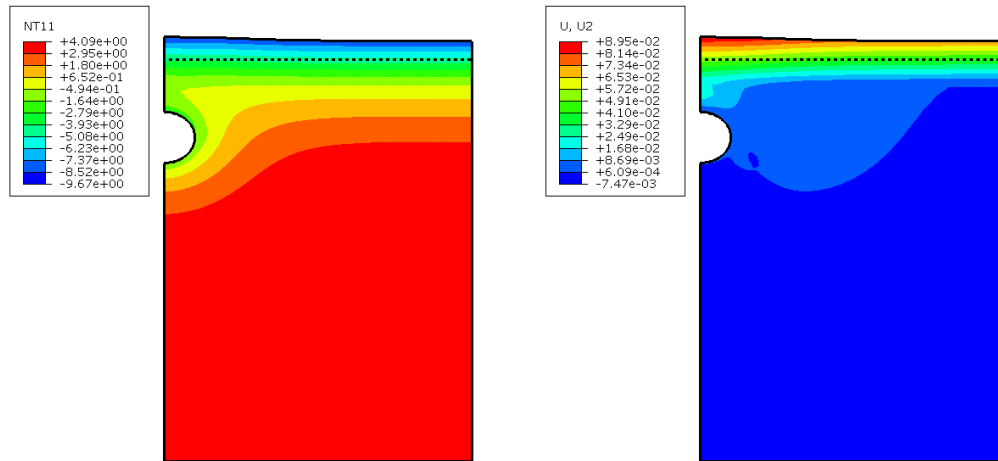


Figure 19. (a) Temperature distribution after 46 days, and (b) frost heave contour (culvert with outside thermal insulation around the circumference, $\lambda = 0.02 \text{ W}/(\text{m } ^\circ\text{C})$).

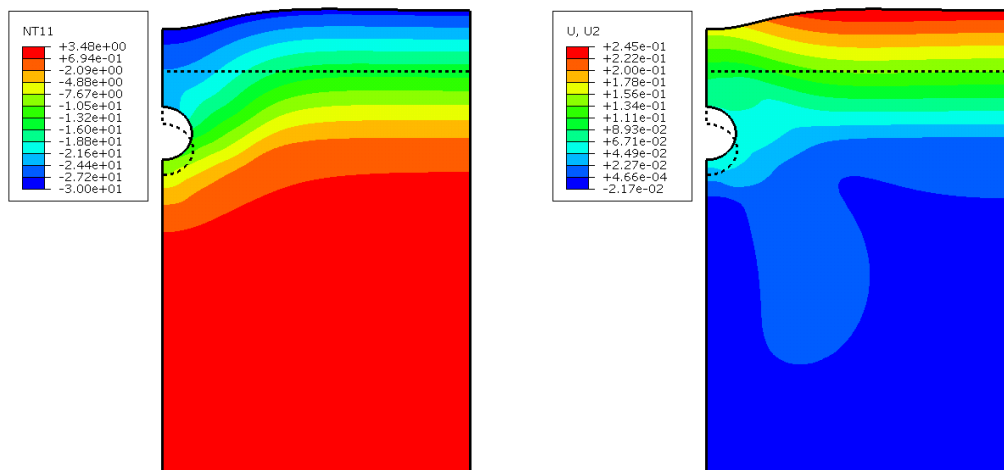


Figure 20. (a) Temperature distribution after 100 days, and (b) frost heave contour (culvert with outside thermal insulation around the circumference, $\lambda = 0.02 \text{ W}/(\text{m } ^\circ\text{C})$).

The results of frost heave simulation around culvert with thermal insulation are shown in Figure 19 and Figure 20. In Figure 19, the maximum “bump” is formed at about 46 days, and the frost heave is smaller compared to that in Figure 17. However, the “depression” in Figure 20 is as large as that in Figure 18.

5 Elasto-plastic constitutive model for freezing and thawing soils

5.1 The model

Little effort was devoted in the past to constitutive modeling of soils subjected to freezing and thawing, and no reliable models have been developed, so far. After 1980's some effort was made toward describing reversible and irreversible deformation, but these efforts did not give rise to computational tools that could be used in model-based simulations. Most of the models were based on continuum approach, and were suited for one type of frozen soil. The changes in strength due to varying soil composition upon freezing and thawing were not addressed by these models. The most recent efforts draw from the area of unsaturated soil mechanics, and they exploit an analogy of cryogenic suction in freezing soil to matric suction in unsaturated soils (e.g., Shastri and Sanchez, 2012; Nishimura, et al., 2009). The development of a model that accounts for deformation and strength evolution caused by freezing and thawing was part of this project, and it was motivated by the absence of models that could be effectively used in model-based simulations

The model developed introduces *ice ratio* e_i as a key parameter in the description of the behavior of the frozen soil. The ice ratio is defined as

$$e_i = \frac{V_i}{V_s} \quad (6)$$

where V_i is the volume of ice and V_s is the volume of the solid constituent (mineral skeleton) in a given volume of soil. Ice ratio e_i is uniquely related to the unfrozen water content (see equation (4))

$$e_i = (w_0 - w) \cdot \frac{\rho_s}{\rho_w} 1.09 \quad (7)$$

where w_0 is the moisture content of saturated soil before freezing, w is the current unfrozen moisture content, and ρ_s and ρ_w are the density of the mineral of the skeleton and water, respectively. Specific volume v and mean stress p are introduced

$$v = \frac{V}{V_s} = 1 + e, \quad p = \frac{1}{3} \sigma_{kk} \quad k = 1, 2, 3 \quad (8)$$

where V is the total volume of the soil, e is the void ratio, and σ_{kk} is the first invariant of the stress state. Compression tests on frozen soils indicate that the behavior can be represented by the normal compression line (NCL) in the $v, \ln p$ plane, and the unloading-reloading line (URL) (Qi et al., 2010, Lee et al., 2002). The slopes of these lines vary,

and they depend on the extent of freezing. The slopes for the two lines are defined by coefficients λ and κ for unfrozen soil, and λ_f and κ_f for frozen soil, respectively. The specific volume upon isotropic compression of frozen soil is given by

$$v = v_f - \lambda_f \ln p \quad (9)$$

and the elastic behavior in unloading-reloading regime is given by

$$\delta v^e = -\kappa_f \frac{\delta p}{p} \quad (10)$$

In the model developed, both λ_f and κ_f are functions of ice ratio e_i . The yield condition of frozen soil is described here with an ellipse in the deviatoric-mean stress plane (q, p), and its analytical expression is presented later in equation (19). Such a surface has been in use for quite some time in the framework of the critical state soil mechanics, and because of its effectiveness and relative simplicity, it was adopted in this constitutive modeling effort. This function has two material parameters: slope M of the critical line, and preconsolidation pressure p_0 . Soils become stronger upon freezing, which is characterized in the developed model by increasing preconsolidation stress p_0 . At the same time, inclinations of NCL and URL lines become flatter in the $v, \ln p$ space. A reasonable relative position of normal compression lines for a soil in both unfrozen state and frozen state is shown in Figure 21(a). The relationship between preconsolidation stress p_0 and ice ratio is illustrated in Figure 21(b). The yield surface and its evolution with ice ratio e_i is illustrated in Figure 21(b) (p_0 is the preconsolidation stress for unfrozen soil, and p_0^f is the preconsolidation stress for the same soil in frozen state with the ice ratio of $e_i = e_{iC}$, p_0^r is a reference stress).

Consider freezing and loading path B-C-D as illustrated in Figure 21. A virgin unfrozen (saturated) soil at state characterized by point B is subjected to freezing under a constant isotropic stress. The specific volume increases due to the volumetric expansion upon phase change. Then, isotropic load is added at constant temperature until point D is reached on the isotropic stress yield line for the frozen soil. During the isotropic loading the ice ratio remains constant, $e_i = e_{iC}$. This is because the ice ratio is related to the unfrozen water content in non-segregation freezing process, thus having a unique relationship to the temperature.

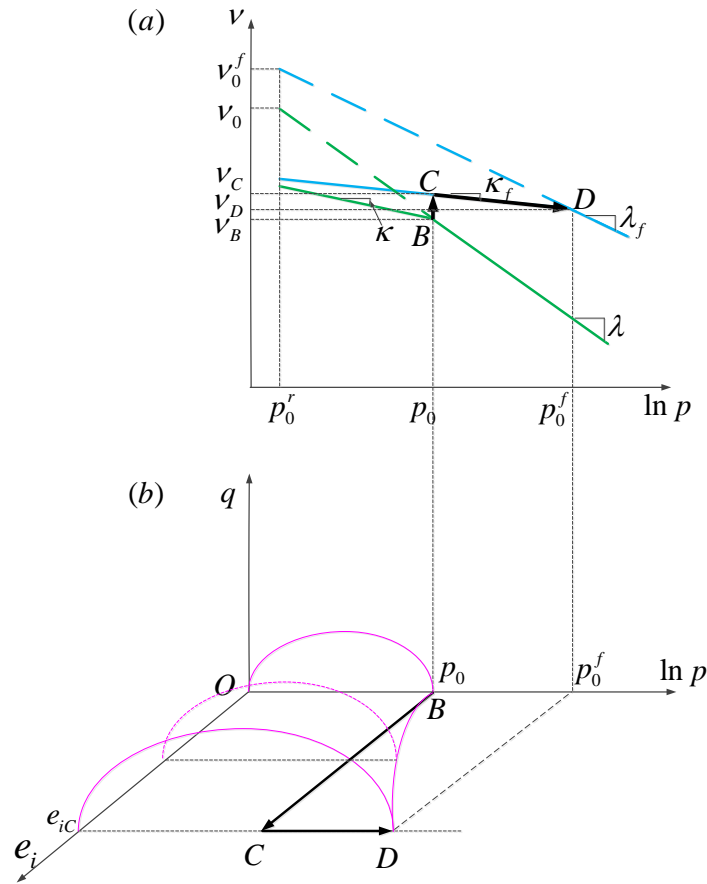


Figure 21. (a) Freeze-thaw thermal loading path in v - $\ln(p)$ plane; (b) “pseudo preconsolidation pressure” changing along BD due to increasing pore ice ratio

Points B and D belong to the same yield curve on p, e_i -plane. Yield stresses p_0^f for frozen states with different ice ratio e_i during freezing from point B to C are located on this curve.

The specific volume at the final point D can be described as

$$v_D = v_B + \Delta v_{BC} - \Delta v_{CD} \quad (11)$$

where Δv_{BC} and Δv_{CD} are the increments due to initial freezing and due to subsequent loading.

The expansion upon freezing is related to phase change and is treated as reversible (it reversed during thawing). This volume change can then be calculated as

$$\Delta v_f = 0.09 e_i \quad (12)$$

Substituting equations (9), (10), and (12) into (11), one obtains

$$v_0^f - \lambda_f \ln \frac{p_0^f}{p_0^r} = (v_0 - \lambda \ln \frac{p_0}{p_0^r}) + 0.09 e_i - \kappa_f \ln \frac{p_0^f}{p_0} \quad (13)$$

where p_0^r is the reference pressure to locate the virgin compression lines for both soil states. Consequently, the increase in isotropic yield stress caused by the ice ratio increase is found as

$$\frac{p_0^f}{p_0^r} = e^{\frac{v_0^f - v_0 - 0.09 e_i}{\lambda_f - \kappa_f}} \left(\frac{p_0}{p_0^r} \right)^{\frac{\lambda - \kappa_f}{\lambda_f - \kappa_f}} \quad (14)$$

The slopes of the NCL and URL of frozen soil are both functions of e_i . Because the frozen soil has limited tendency for compression (pores are filled with ice), slope λ_f drops dramatically compared to that for the unfrozen soil. The following relationship is postulated

$$\lambda_f = \lambda \exp(-\alpha e_i) \quad (15)$$

where α is a soil constant. κ_f is assumed to be constant during freezing, i.e., $\kappa_f = \kappa$.

In order for equation (14) to yield p_0 for unfrozen soil when $e_i = 0$, we postulate the following linear law defining the shift of v_0 to v_0^f as a function of e_i

$$v_0^f = v_0 - (\beta - 0.09) e_i \quad (16)$$

where β is a soil constant (to be determined from calibration). Equation (14) can, therefore, be written as

$$\frac{p_0^f}{p_0^r} = e^{\frac{-\beta e_i}{\lambda_f - \kappa_f}} \left(\frac{p_0}{p_0^r} \right)^{\frac{\lambda - \kappa_f}{\lambda_f - \kappa_f}} \quad (17)$$

The plastic volumetric strain due to mechanical load and the thermal process is then described in the following expression

$$d\varepsilon_v^{pl} = \frac{\lambda_f - \kappa_f}{v} \frac{dp_0^f}{p_0^f} = \frac{\lambda - \kappa_f}{v} \frac{dp_0}{p_0} \quad (18)$$

The yield function in the model is similar to that in Cam clay model, but with the preconsolidation pressure p_0 dependent on ice ratio e_i

$$f = q^2 - M^2 p [p_0(e_i) - p] = 0 \quad (19)$$

An associate flow rule is assumed to describe plastic deformation (i.e., the plastic potential $g = 0$ had the same form as $f = 0$).

Thawing of a frozen soil decreases the amount of ice in pores, reduces “ice cementation” and, consequently, reduces the strength. For non-segregation frozen soils, the strength after complete thawing tends to move back to the same envelope as before freezing. There will be no further weakening since no thermally induced mass migration occurred during freezing, and the change of the soil fabric during the thermal process was not significant.

5.2 Thermal-mechanical load process

To illustrate the model, a freeze-thaw cycle along with an external load applied is shown in Figure 22. The thermal process is depicted with the blue (freezing) and red (thawing) lines, whereas the mechanical loading-unloading is depicted by the green lines.

A saturated soil specimen is preconsolidated under isotropic compression from point A to B. Then, under constant stress, the freezing process takes place (B-C), and the ice ratio at point C is e_{iC} . In this process, the isotropic yield stress (apparent preconsolidation stress for corresponding frozen soil) increases from B_1 to D_1 following equation (14), and it has a value of p_0^D at point D_1 (the soil has the same apparent preconsolidation stress after it had been frozen at point C_1). The below-freezing temperature is then maintained, and isotropic compression is increased to reach the normal compression line for frozen soil at pressure p_0^D ; the load is then continued along the NCL to reach p_0^E . During this loading, the void ratio e is changing while the ice ratio remains constant. This is based on an assumption that ice and soil skeleton are both incompressible. From C to D, the frozen soil experiences elastic behavior, whereas from D to E it behaves plastically.

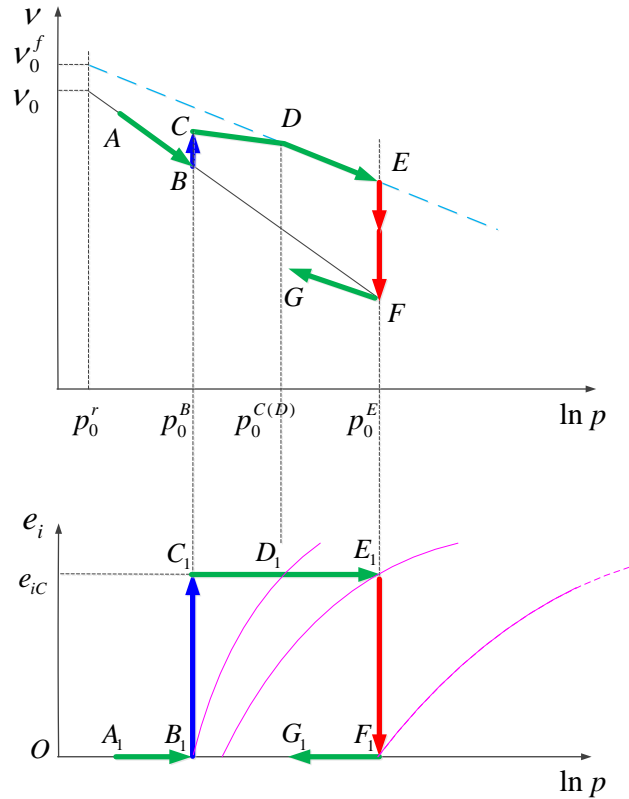


Figure 22. Freeze-thaw cycle and load path with corresponding yield curves

Thereafter, the soil is thawed at constant stress p_0^E . Once ice starts melting, the soil can no longer sustain load $p = p_0^E$, and the process of consolidation will start, moving the soil to the normal compression line for the unfrozen soil (point F). Unloading from F results in an elastic rebound along the URL for unfrozen soil to G.

5.3 Implementation and application of the model

The constitutive model was implemented into the finite element system ABAQUS using subroutine UMAT and UEXPAN to solve boundary value problems.

The model was calibrated based on the tests done by Qi, et al. (2010). Parameters obtained from curve fitting into the test data are listed in Table 5. The corresponding preconsolidation stress curve with freezing temperature is shown in Figure 23.

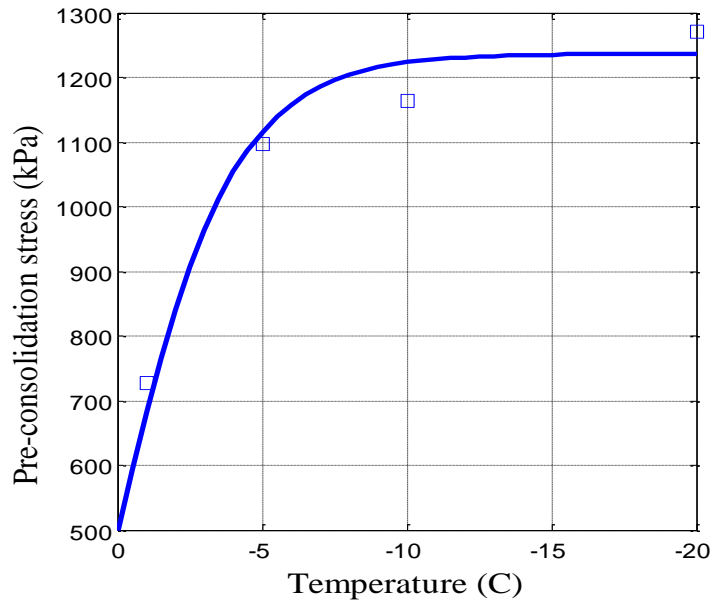


Figure 23. Calibration of preconsolidation stress for frozen soil vs temperatures

Table 5 Parameters and initial values in simulation

| λ | κ | p_0^{start} | M | α | β |
|-----------|----------|-----------------|------|----------|---------|
| 0.15 | 0.03 | 60 (kPa) | 1.0 | 0.225 | 0 |
| e_0 | w^* | $\bar{w} = w_0$ | a | μ | |
| 0.85 | 0.08 | 0.325 | 0.45 | 0.3 | |

The parameters λ and κ are the slopes for NCL and URL lines in compression plane. M is the slope for the critical state line. p_0^{start} and e_0 are the initial values for the preconsolidation pressure and the void ratio. w^* , \bar{w} , and a are parameters for unfrozen water content function.

To illustrate the response of the model to loading and thermal changes, a soil column subjected to both the mechanical load and a thermal process was simulated. The soil column is 0.07 m in height. The vertical walls of the column are adiabatic and rigid. The initial uniform temperature is 1°C, and the initial vertical and horizontal compressive stresses are 20 kPa and 10 kPa, respectively. Initial and boundary conditions in terms of load and temperature at the top of the column are shown in Figure 24. The bottom of the column is fixed and the temperature is maintained at 1°C throughout the process. The temperature distribution at $t = 0$ and $t = 300$ h are shown in Figure 25. More details on this simulation can be found in Zhang and Michalowski (2013).

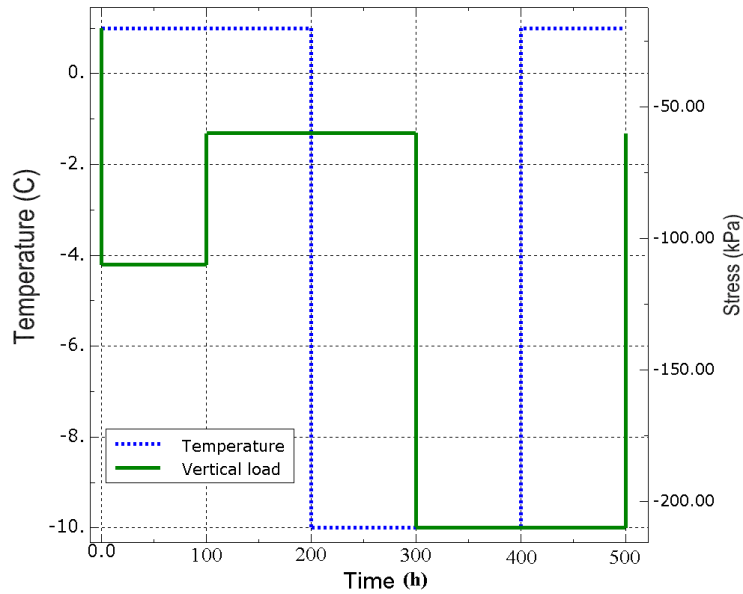


Figure 24. Boundary condition on top of the soil column

The relationship between void ratio and the vertical stress is shown in Figure 26 for element #18 and #4. For element #18, the temperature is about -4.5°C when the column reaches steady state after freezing, having more pore ice and being stronger than element #4 whose steady state temperature is around -0.3°C . There is a substantial difference in the behavior of the two elements during the load segment from 60 to 210 kPa: while element #18 behaves elastically, element #4 is elastic only until the load reaches 160 kPa, and becomes elasto-plastic afterward. Both elements experience additional settlement due to thawing.

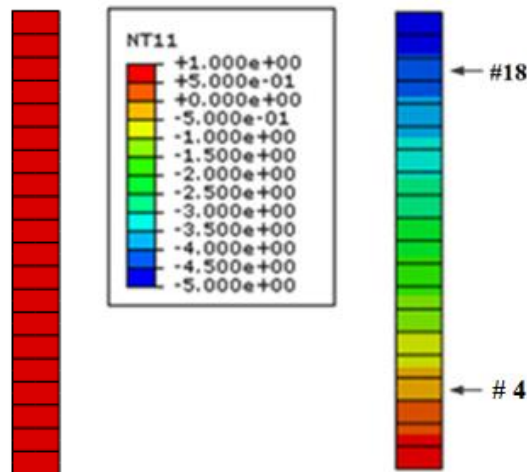


Figure 25. Temperature distribution at $t = 0$ and $t = 300$ h

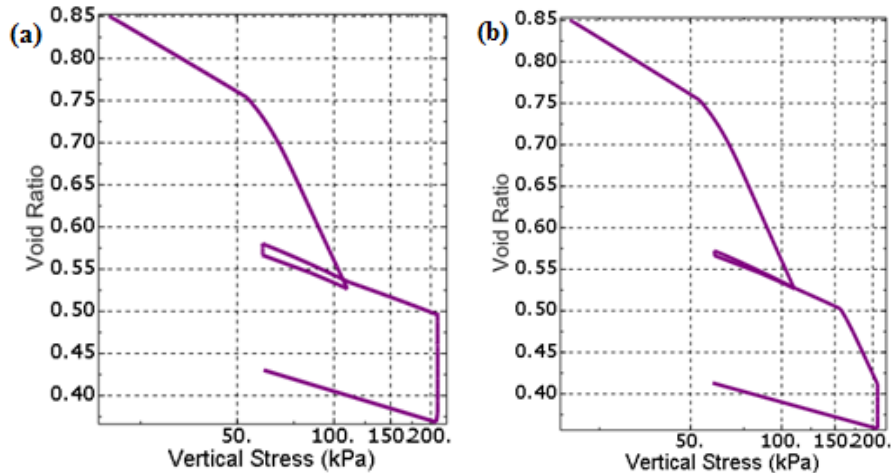


Figure 26. Compression for element #18 (a) and element #4 (b)

Other boundary value problems were also simulated using the model developed. These are not presented here, but will be a subject of future publications.

6 Summary of the most important results

The principal contribution of this research is the development of the model for simulating freezing-thawing cycles in frost-susceptible soils. The model is capable of simulating frost heave very effectively, and the authors view it as the most efficient of existing models. This model also addresses the problem of soil thawing. This work is a pioneering effort to account for the changes in soil strength associated with thawing, and predictions of thaw weakening.

REFERENCES

- Aitken, G. W. and Fulwider, C. W. (1962). "Ground temperature observations, Aniak, Alaska." *U.S. Army Cold Region Research and Engineering Laboratory, Corps of Engineers*, Hanover, New Hampshire, 10.
- Andersland, O. B. and Ladanyi, B. (2004). "Frozen ground engineering." Wiley, New Jersey, 102 - 119.
- Fukuda, M., Kim H. and Kim Y. (1997). "Preliminary results of frost heave experiments using standard test sample provided by TC8." *Proceedings of the International Symposium on Ground Freezing and Frost Action in Soils*, Luleå Sweden, 25 - 30.
- Huang S.L., Bray M.T., Akagawa S., and Fukuda M. (2004). "Field investigation of soil heave by a large diameter chilled gas pipeline experiment, Fairbanks, Alaska." *Journal of Cold Regions Engineering*, 18 (1), 2-34.
- Lai, Y., Long, J. and Xiaoxiao, C. (2009). "Yield criterion and elasto-plastic damage constitutive model for frozen sandy soil." *Int. J. Plasticity*, 25, 1177-1205.

- Lee M.Y., Fossum A., Costin L.S. and Bronowski D. (2002). "Frozen soil material testing and constitutive modeling." *Sandia National Laboratories Report 2002-0524*.
- Kim, K. (2011). "Multi-dimensional frost heave modeling with SP porosity growth function." PhD Thesis, University of Alaska, Fairbanks.
- Michalowski, R.L. (1993). "A constitutive model of saturated soils for frost heave simulations." *Cold Regions Science and Technology*, 22(1), 47-64.
- Michalowski, R. L. and Zhu, M. (2006). "Frost heave modeling using porosity rate function." *International Journal for Numerical and Analytical Methods in Geomechanics*, 30, 703 - 722.
- National Climate Data Center, Retrieved June 18, 2011, Record of Climatological Observations, from <http://cdo.ncdc.noaa.gov/dly/DLY>.
- Nishimura S., Gens A., Olivella S. and Jardine R. J. (2009). "THM-coupled finite element analysis of frozen soil: formulation and application". *Géotechnique*, 59(3), 159-171.
- Qi J., Hu W. and Ma W. (2010). "Experimental study of a pseudo-preconsolidation pressure in frozen soils." *Cold Regions Science and Technology*, 60, 230-233.
- Selvadurai, A. P. S., Hu, J. and Konuk, I. (1999). "Computational modeling of frost heave induced soil-pipeline interaction, II. Modelling of experiments at the Caen test facility". *Cold regions science and technology*, 29, 229 - 257.
- Shastri A. and Sanchez M. (2012.) "Mechanical modeling of frozen soils incorporating the effect of cryogenic suction and temperature." *GeoCongress 2012: State of the Art and Practice in Geotechnical Engineering*, 2492-2501.
- Wei L., Hong F. and He W. (2011.) "Research on visco-elastic-plastic creep model of artificially frozen soil under high confining pressures." *Cold Regions Science and Technology*, 65 (2), 219-225.
- Williams, P. J. and Smith, M. W. (1989). "The Frozen Earth". *Fundamentals of Geocryology*, Alden Press, Oxford, 89 - 90.
- Zhang, Y. and Michalowski, R.L (2012). "Frost-induced heaving of soil around a culvert." 2012 ASCE Geo-Congress, Oakland, CA, March 25-29.
- Zhang, Y. and Michalowski, R.L (2013). "Constitutive model and simulation of non-segregation freezing and thawing in soils." Proc. 18th *International Conference on Soil Mechanics and Geotechnical Engineering*, Paris 2013.